

# QUANTUM CIRCUIT COMPLEXITY FOR LINEARLY POLARISED LIGHT

EVALDO M. F. CURADO<sup>a,b</sup>, SOFIANE FACI<sup>c</sup>, JEAN-PIERRE GAZEAU<sup>d</sup>,  
TOMOI KOIDE<sup>e</sup>, ALAN C. MAIOLI<sup>a</sup>, AND DIEGO NOGUERA<sup>a</sup>

**ABSTRACT.** In this study, we explore a form of quantum circuit complexity that extends to open systems. To illustrate our methodology, we focus on a basic model where the projective Hilbert space of states is depicted by the set of orientations in the Euclidean plane. Specifically, we investigate the dynamics of mixed quantum states as they undergo interactions with a sequence of gates. Our approach involves the analysis of sequences of real  $2 \times 2$  density matrices. This mathematical model is physically exemplified by the Stokes density matrices, which delineate the linear polarisation of a quasi-monochromatic light beam, and the gates, which are viewed as quantum polarisers, whose states are also real  $2 \times 2$  density matrices. The interaction between polariser-linearly polarised light is construed within the context of this quantum formalism. Each density matrix for the light evolves in an approach analogous to a Gorini-Kossakowski-Lindblad-Sudarshan (GKLS) process during the time interval between consecutive gates. Notably, when considering an upper limit for the cost function or tolerance or accuracy, we unearth that the optimal number of gates follows a power-law relationship.

---

*Date:* October 7, 2024.

## CONTENTS

1. Introduction	4
2. Quantum formalism for the Euclidean plane	9
2.1. Euclidean plane with Dirac notations	9
2.2. Pure and mixed states	10
2.3. Time evolution	12
3. Example of mixed states: linear polarisation of light and Stokes parameters	15
4. Polarisation of the light through a von Neumann quantum interaction	18
4.1. Outcomes of interaction with quantum polariser	18
4.2. Light after interaction	20
5. Classical polarisation of the light versus quantum formalism	22
6. General setting for quantum circuits in the plane	24
6.1. GKLS equations	24
6.2. Metric structure of mixed states for the Euclidean plane	25
7. Some analytic solutions to GKLS equations	27
7.1. Constant energy $\mathcal{E}$	27
7.2. Constant angle $\phi$	29
7.3. Constant $\dot{\phi}$	30
8. Numerical approach to complexity circuit	30
9. Conclusion	35
Appendix A. Density matrix for light after polarisation interaction	38
Appendix B. Quantum polariser after interaction	39
Appendix C. Infinitesimal evolution after interaction	39
Acknowledgments	41

## References

41

## I. INTRODUCTION

In the realm of computer science, computational complexity (see for instance the inspiring introduction in [1], and references therein) pertains to the smallest number of operations required to accomplish a specific task.

Quantum computation relies on a sequence of logic gates, each interacting with only a small number of qubits. This sequence defines the evolution operator implemented by the computer. Ideally, this operator is unitary if the system is closed; however, in more realistic scenarios, it may describe the dynamics of an open system.

The difficulty of performing the computation is determined by the number of gates the algorithm utilizes. An algorithm is considered efficient if the number of required gates increases only polynomially with the size of the problem being addressed.

In the closed system case, the process commences by establishing a “reference” quantum state denoted as  $|\psi_R\rangle$ , within the framework of some Hilbert space  $\mathcal{H}$ . Following this, one proceeds to generate a unitary transformation  $U$ , which, through its operation, yields the desired “target” state, represented as

$$(I.1) \quad |\psi_T\rangle = U|\psi_R\rangle.$$

This transformation is essential in achieving the intended outcome.

The unitary transformation  $U$  is assembled using a specific set of elementary or universal gates. These gates are applied in sequence to the initial state to tentatively attain the target state. In the context of finite discrete operations this objective is, in general, not achieved,  $|\psi_T\rangle \neq U|\psi_R\rangle$ . Consistently, an introduced parameter, known as “tolerance” or “accuracy”, often marked as  $\epsilon$ , becomes crucial. This parameter allows

for a certain margin of error, acknowledging that achieving exact equality might not always be possible. Instead, the success of the transformation is determined by the degree of proximity between the two states, as measured by a designated distance metric. In other words, the transformation can be considered successful if the two states are sufficiently close, even if they are not precisely equal.

$$(1.2) \quad \|\lvert\psi_T\rangle - U\lvert\psi_R\rangle\| \leq \epsilon.$$

Here comes the subtlety of computational complexity. Eq. (1.2) quantifies how hard it is, given one state, to make another, and this cannot always be expressed through the usual inner product of the Hilbert space of states. Even for a single two-state system the computational complexity is rich, see [2, 3] for an extensive discussion. The idea of complexity geometry translates the fact that some controlled operations are harder to perform, such as gates touching many qubits at the same time. Even for a single qubit some elementary universal gates might be harder to implement than others. It is therefore worth studying the simplest possible case. Naturally, there won't be a singular circuit that accomplishes the desired transformation described in Eq. (1.1). In most cases, there will be an abundance of gate sequences that yield the same target state. Nevertheless, the *complexity* of the state  $\lvert\psi_T\rangle$  can be defined as the *smallest* quantity of gates essential to effect the transformation in Eq. (1.1) (in fact it is the relative complexity between the reference and target states that matters). This definition encapsulates the number of elementary gates within the most efficient or shortest circuit. Consequently, the challenge lies in discerning this optimal circuit from the myriad of conceivable alternatives.

Nielsen et al [4, 5, 6] tackled these questions using a geometric approach inspired by the theory of optimal quantum control and introducing a cost function to evaluate the different feasible paths. Their work draws upon concepts from papers such as those by Gordon and Rice (1997) [7], Shapiro and Bruner (2003) [8], Rabitz et al (2000) [9], and Rice and Zhao (2000) [10].

Building upon the insights drawn from these concepts, and taking cues from recent studies like those mentioned in [11] and [12], our work delves into a form of quantum circuit complexity that extends to open systems. It is natural to take into account the influence of the environment, no matter how negligible it might be. In this pursuit, we broaden the formalism to a more encompassing level. Indeed, it is very hard to keep a qubit isolated and in fact dissipate very quickly. Better understanding the dynamics of how this happens and the complexity geometry of open systems is thus fundamental, see for instance [13].

Specifically, we investigate the evolution of mixed quantum states as they undergo interactions with a sequence of gates. Notably, in contrast to the unitary paradigm described in Eq. (1.1), our approach deals with a sequence, denoted as  $(\rho_n)_{0 \leq n \leq N-1}$ , consisting of  $N$  density matrices. Each of these matrices evolves within the framework of a Gorini-Kossakowski-Lindblad-Sudarshan (GKLS) process during the time interval between two consecutive gates. To exemplify our approach, we consider a foundational scenario where the Hilbert space of states is the elementary Euclidean plane  $\mathbb{R}^2$ . The corresponding mixed states  $\rho$  are of the form

$$(1.3) \quad \rho_{r,\phi} = \frac{1}{2} \begin{pmatrix} 1 + r \cos 2\phi & r \sin 2\phi \\ r \sin 2\phi & 1 - r \cos 2\phi \end{pmatrix},$$

with  $r \in [0, 1]$ ,  $\phi \in [0, \pi]$ . Pure states correspond to  $r = 1$ , *i.e.*,  $\rho_{1,\phi} = \begin{pmatrix} \cos \phi \\ \sin \phi \end{pmatrix} \begin{pmatrix} \cos \phi & \sin \phi \end{pmatrix} \equiv |\phi\rangle\langle\phi|$ , and  $r = 0$  is for totally mixed states, *i.e.*,  $\rho_{0,\phi} = \mathbb{1}_2/2$ . This example offers a significant advantage in that it lends itself to straightforward implementation of both analytical calculations and numerical simulations.

Hence, we start from a reference state  $\rho_{r_R, \phi_R}$  and aim at reaching the target state  $\rho_{r_T, \phi_T}$  through a sequence of  $N$  gates which modify parameters  $r, \phi$  and leave the mixed state to interact with its dissipative environment till the next gate. We adopt a von Neumann model of interaction with the gate, as detailed by von Neumann [14], to describe the interaction between linearly polarised light and a quantum polariser. Here, the term “quantum polariser” refers to a quantum system represented by real  $2 \times 2$  density matrices.

In view of comparing various paths in the space of such density matrices, we will use criteria expressed in terms of euclidean distances between points  $(r, \phi)$  which parameterize density matrices. Moreover, in view of the important outcome of our work, deviating from Nielsen’s criteria will have a negligible impact on our approach.

In Section 2, we expound the application of quantum formalism to the set of orientations (or directions) in the Euclidean plane, treating it as a projective real Hilbert space of quantum states or Dirac kets. Pure and mixed states are expressed as real  $2 \times 2$  matrices, each in a direct and intuitive correspondence with points within the upper half-unit disk. The description of quantum observables follows suit, employing symmetric real  $2 \times 2$  matrices. Subsection 2.3 examines the time evolution of the states discussed earlier. For closed systems, this evolution is governed by simple rotations in the plane. However, when the system interacts

with its environment, the time evolution of the density matrix  $\rho_{r,\phi}$  is governed by the quantum master equation in the GKLS form, which describes open systems.

In Section 3, we showcase a compelling illustration of pure and mixed states, specifically focusing on real  $2 \times 2$  matrices that delineate the linear polarisation of light through Stokes parameters (a comprehensive review of classical and quantum polarisations is given in [15]). This example holds particular significance for our study, infusing a tangible and physical dimension into our exploration of circuit complexity within the confines of the two-dimensional Euclidean framework.

In Section 4, we revisit the above discussion on linear polarisation of light, this time exploring it in the context of the framework of the von Neumann theory of quantum measurement [16]. We describe the evolution of the corresponding (Stokes) density matrix as it interacts with a quantum polariser. This evolution is unitary, indicating that there is no collapse of polarisation along a specific direction, as might be expected with classical polarisation.

In Section 5, we offer a brief overview of the physical properties of classical polarisers and clarify how they relate to the quantum framework of light polarization that we introduced in Section 4.

Section 6 establishes a connection between the previously discussed GKLS equation and the geometric elements such as trace distances between density matrices and the expected straight line geodesic. These connections are essential for carrying out our program of adapting quantum circuit complexity to the evolution of pure or mixed quantum states in the context of the Euclidean plane.

Section 7 provides analytic results enabling us to determine the trajectories derived from the dynamical system presented in the GKLS equation.

The exploration continues in Section 8 with concrete numerical investigations. Here, we introduce an algorithmic approach and evaluate its complexity alongside a specific definition for the distance metric. The outcomes stem from the application of multiple polarisers following a distinct strategy, refining the trajectories to align piecewise with desired geodesics. Notably, we observe that our approach effectively adheres to a power law and holds potential applicability across various system types.

Section 9 presents a comprehensive discussion regarding the significance and future implications of our results.

Appendices A, B and C are dedicated to providing additional technical details that enhance the comprehension of our results.

## 2. QUANTUM FORMALISM FOR THE EUCLIDEAN PLANE

The Euclidean plane, represented as the vector space  $\mathbb{R}^2$  with its standard dot product, serves as one of the straightforward models of a Hilbert space. In this section, we fix the notations and provide an overview of the real two-dimensional quantum formalism that will be elaborated upon in subsequent sections. Although it may seem rudimentary at first glance, this material adeptly unveils a substantial part of subtleties of the quantum formalism.

**2.1. Euclidean plane with Dirac notations.** By adopting the Dirac ket notations, as is shown in Fig. 1, an orthonormal basis of the Euclidean plane  $\mathbb{R}^2$  is defined by the two vectors  $|\hat{i}\rangle$  and  $|\hat{j}\rangle$  such that

$$(2.1) \quad \langle \hat{i} | \hat{i} \rangle = 1 = \langle \hat{j} | \hat{j} \rangle, \quad \langle \hat{i} | \hat{j} \rangle = 0, \quad \mathbb{1}_2 = |\hat{i}\rangle\langle\hat{i}| + |\hat{j}\rangle\langle\hat{j}|$$

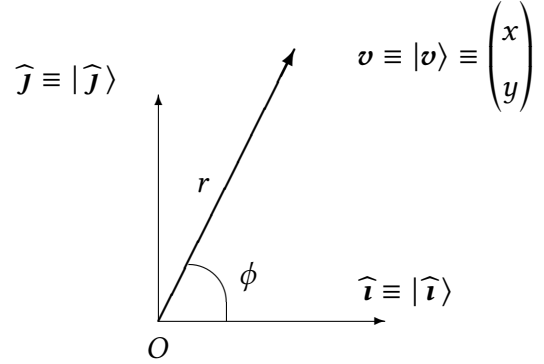


FIGURE 1. Euclidean plane as a vector space of Dirac kets.

$|\psi\rangle$  denotes the vector with length  $r$  and polar angle  $\phi \in [0, 2\pi)$ . For  $r = 1$  the corresponding unit vector is denoted by  $|\phi\rangle$ .

A vector  $|\psi\rangle$  with polar angle  $\phi \in [0, 2\pi)$  determines a sense on its support. The latter is a direction or, synonymously, an orientation in the plane.

## 2.2. Pure and mixed states.

*Pure states.* In the quantum formalism applied to the Euclidean plane, a unit vector positioned at a polar angle  $\phi$  relative to the basis vector  $\hat{i}$  symbolizes the pure state  $|\phi\rangle$ . Its corresponding orthogonal projector reads as

$$(2.2) \quad P_\phi = |\phi\rangle\langle\phi| = \mathcal{R}(\phi)|0\rangle\langle 0|\mathcal{R}(-\phi).$$

Here,  $\mathcal{R}(\phi)$  denotes the matrix of rotation in the plane by the angle  $\phi$ ,

$$(2.3) \quad \mathcal{R}(\phi) = \begin{pmatrix} \cos \phi & -\sin \phi \\ \sin \phi & \cos \phi \end{pmatrix}.$$

$P_\phi$  is commonly referred to as a pure state. This designation is consistent with the fact that the projector ignores sense along the orientation defined by the polar angle  $\phi$ ,  $P_\phi = P_{\phi+\pi}$ .

*Mixed states.* Mixed states or density matrices  $\rho$  are unit trace and non-negative  $2 \times 2$  matrices. Thus, they have a spectral decomposition of the form

$$(2.4) \quad \rho = \frac{1+r}{2} |\phi\rangle\langle\phi| + \frac{1-r}{2} \left| \phi + \frac{\pi}{2} \right\rangle \left\langle \phi + \frac{\pi}{2} \right|$$

where the  $0 \leq r \leq 1$ . Hence we can write  $\rho$  in terms of the polar coordinates  $(r, \phi)$  of a point in the upper half unit disk:

$$(2.5) \quad \begin{aligned} \rho \equiv \rho_{r,\phi} &= \begin{pmatrix} \frac{1}{2} + \frac{r}{2} \cos 2\phi & \frac{r}{2} \sin 2\phi \\ \frac{r}{2} \sin 2\phi & \frac{1}{2} - \frac{r}{2} \cos 2\phi \end{pmatrix} \\ &= \frac{1}{2} (\mathbb{1}_2 + r \mathcal{R}(\phi) \sigma_3 \mathcal{R}(-\phi)) , \end{aligned}$$

with  $\sigma_3 = \begin{pmatrix} 1 & 0 \\ 0 & -1 \end{pmatrix}$ . The matrix  $\rho$  is  $\pi$ -periodic in variable  $\phi$ ,  $\rho_{r,\phi} = \rho_{r,\phi+\pi}$ , and we check that for  $r = 1$  it is just the orthogonal projector on the unit vector  $|\phi\rangle$  with polar angle  $\phi$ , i.e.  $\rho_{1,\phi} = P_\phi$ . Also note the covariance property of  $\rho_{r,\phi}$  trivially deduced from Eq. (2.5):

$$(2.6) \quad \mathcal{R}(\theta) \rho_{r,\phi} \mathcal{R}(-\theta) = \rho_{r,\phi+\theta} .$$

The parameter  $r$  can be viewed as a measure of the distance of  $\rho$  to the pure state  $P_\phi$  while  $1 - r$  measures the degree of “mixing”. A statistical interpretation is made possible through the von Neumann entropy [17] defined as

$$(2.7) \quad S_\rho := -\text{Tr}(\rho \ln \rho) = -\frac{1+r}{2} \ln \frac{1+r}{2} - \frac{1-r}{2} \ln \frac{1-r}{2} .$$

As a function of  $r \in [0, 1]$   $S_\rho$  is nonnegative, concave and symmetric with respect to its maximum value  $\log 2$  at  $r = 0$ , *i.e.*,  $\rho_0 \equiv \mathbb{1}_2/2$ , which describes the state of completely random orientations, while a pure state  $r = 1$  yields a vanishing entropy.

*Quantum observables.* A quantum observable,  $A$  is represented by a  $2 \times 2$  real symmetric matrix, *i.e.*, a self-adjoint operator. Its spectral decomposition in terms of the two orthogonal projectors associated with its real eigenvalues reads:

$$(2.8) \quad A = \lambda_{\parallel} P_\gamma + \lambda_{\perp} P_{\gamma+\pi/2}.$$

Three basic matrices generate the Jordan algebra of all real symmetric  $2 \times 2$  matrices. They are the identity matrix  $\mathbb{1}_2$  and the two real Pauli matrices,

$$(2.9) \quad \sigma_1 = \begin{pmatrix} 0 & 1 \\ 1 & 0 \end{pmatrix}, \quad \sigma_3 = \begin{pmatrix} 1 & 0 \\ 0 & -1 \end{pmatrix}.$$

### 2.3. Time evolution.

**2.3.1. Closed systems.** When is applied to a possibly time-dependent quantum observable  $A(t)$  the Heisenberg-Dirac equation reads as

$$(2.10) \quad i \frac{d}{dt} A_H = [A_H, H(t)] + U(t, t_0)^\dagger \left( i \frac{\partial}{\partial t} A \right) U(t, t_0),$$

where  $A_H(t) := U(t, t_0)^\dagger A(t) U(t, t_0)$ . As representing a physical quantity, namely the energy of the system, the Hamiltonian  $H(t)$  is a self-adjoint operator and generates the unitary evolution operator  $i \frac{\partial}{\partial t} U(t, t_0) = H(t) U(t, t_0)$ . In the present context one easily checks [11] that the allowed form of this Hamiltonian reads:

$$(2.11) \quad H(t) = \begin{pmatrix} 0 & -i\mathcal{E}(t) \\ i\mathcal{E}(t) & 0 \end{pmatrix} \equiv i\mathcal{E}(t)\tau_2,$$

where the matrix  $\tau_2$  is defined in terms of the second Pauli matrix by

$$(2.12) \quad \tau_2 = -i\sigma_2 = \begin{pmatrix} 0 & -1 \\ 1 & 0 \end{pmatrix}.$$

As expected, the corresponding evolution operator acts as a rotation in the plane.

$$(2.13) \quad U(t, t_0) = \exp i \int_{t_0}^t H(t') dt' = \mathcal{R} \left( \int_{t_0}^t \mathcal{E}(t') dt' \right).$$

Since the Heisenberg-Dirac equation is homogeneous in the imaginary  $i$ , we can describe this dynamics in terms of real numbers only. We just have to deal with the real pseudo-Hamiltonian (actually there is no phase space here!):

$$(2.14) \quad \tilde{H}(t) = \begin{pmatrix} 0 & -\mathcal{E}(t) \\ \mathcal{E}(t) & 0 \end{pmatrix} = \mathcal{E}(t) \tau_2.$$

One finally obtains the Majorana-like equation, where only real numbers are involved:

$$(2.15) \quad \frac{dA_H}{dt} = [A_H, \tilde{H}(t)] + U(t, t_0)^\dagger \left( \frac{\partial A}{\partial t} \right) U(t, t_0),$$

On the algebraic side, we note that our real quantum dynamics involves the antisymmetric matrix  $\tau_2$ . Together with  $\sigma_1$  and  $\sigma_3$  these 3 matrices generate the Lie algebra  $\mathfrak{sl}(2, \mathbb{R})$  of the group  $SL(2, \mathbb{R})$  of  $2 \times 2$  real matrices with determinant equal to 1.

$$(2.16) \quad [\sigma_1, \tau_2] = 2\sigma_3, \quad [\tau_2, \sigma_3] = 2\sigma_1, \quad [\sigma_3, \sigma_1] = -2\tau_2.$$

**2.3.2. GKLS Open systems for  $\mathbb{R}^2$ .** Restricting the form of “acceptable” Hamiltonians to Eq. (2.11) or Eq. (2.14) is not tenable since this family does not include the case of quantum *open* systems, particularly when the latter is submitted to measurement. Hence we consider an extension

of Eq. (2.15) to a type of *quantum master* equation, namely the Gorini-Kossakowski-Lindblad-Sudarshan (GKLS) equation [18], often just named Lindblad equation [19], describing the time evolution of the density matrix  $\rho_{r,\phi}$  in Eq. (2.5) for an open system. When applied to the evolution of a quantum observable  $A$ , the GKLS equation in its diagonal form (which does not restrict its validity) is expressed as

$$(2.17) \quad \frac{dA}{dt} = i[H, A] + \sum_k h_k \left[ L_k A L_k^\dagger - \frac{1}{2} (A L_k^\dagger L_k + L_k^\dagger L_k A) \right] \equiv \mathcal{L}(A),$$

where the  $L_k$ 's together with the identity form an arbitrary basis of operators and the coefficients  $h_k$  are non-negative constants. In the present framework with no imaginary  $i$  the three matrices  $\sigma_1, \tau_2, \sigma_3$ , together with the identity form a basis for the vector space of real  $2 \times 2$  matrices; then the above equation, when applied to  $\rho_{r,\phi}$ , becomes

$$(2.18) \quad \begin{aligned} \frac{d\rho_{r,\phi}}{dt} &= [\rho_{r,\phi}, \tilde{H}] + h_1 (\sigma_1 \rho_{r,\phi} \sigma_1 - \rho_{r,\phi}) + h_2 (-\tau_2 \rho_{r,\phi} \tau_2 + \rho_{r,\phi}) + h_3 (\sigma_3 \rho_{r,\phi} \sigma_3 - \rho_{r,\phi}) \\ &= r \left( \frac{\mathcal{E}(t)}{\hbar} \sin 2\phi - h_1 \cos 2\phi \right) \sigma_3 + r \left( -\frac{\mathcal{E}(t)}{\hbar} \cos 2\phi - h_3 \sin 2\phi \right) \sigma_1 + h_2 \mathbb{1}_2. \end{aligned}$$

Since  $\frac{d\rho_{r,\phi}}{dt} \equiv \dot{\rho}_{r,\phi} = \frac{1}{2}(\dot{r} \cos 2\phi - 2r \sin 2\phi \dot{\phi})\sigma_3 + \frac{1}{2}(\dot{r} \sin 2\phi + 2r \cos 2\phi \dot{\phi})\sigma_1$ , we infer that  $h_2 = 0$ , and, by identification, one reaches the first-order differential (dynamical) system

$$(2.19) \quad \dot{\phi} = \alpha \sin 4\phi - \mathcal{E}(t), \quad \alpha := \frac{h_1 - h_3}{2} \in \mathbb{R},$$

$$(2.20) \quad \frac{\dot{r}}{r} = -2\alpha \cos 4\phi - \beta, \quad \beta := h_1 + h_3 > 0.$$

Eq. (2.19) leads to a kind of Riccati equation [20]. Having in hand a solution  $\phi(t)$ , Eq. (2.20) is easily integrated and we find

$$(2.21) \quad r(t) = r_0 \exp \left[ -\beta(t - t_0) - 2\alpha \int_{t_0}^t \cos 4\phi(t') dt' \right].$$

Due to the positiveness of  $\beta$ , we infer that  $r \rightarrow 0$ , i.e.,  $\rho_{r,\phi} \rightarrow \mathbb{1}_2/2$  as  $t \rightarrow \infty$ , which means that the von Neumann entropy of the open system tends to its maximum at large time, as we can expect. Note that for  $\alpha = 0$  the angle  $\phi$  behaves like for a closed system,

$$(2.22) \quad \phi(t) - \phi(t_0) = - \int_{t_0}^t dt' \mathcal{E}(t'),$$

whereas the behaviour of  $r$  simplifies to  $r(t) = r_0 e^{-2h_1(t-t_0)}$ .

### 3. EXAMPLE OF MIXED STATES: LINEAR POLARISATION OF LIGHT AND STOKES PARAMETERS

A well-established physical interpretation of  $2 \times 2$  real or complex density matrices is found in the context of the Stokes parameters, which characterize the polarization of light. This interpretation is thoroughly explored in [21] and related references. For a detailed discussion on the significance and measurement of these parameters, see [22].

Drawing inspiration from Landau and Lifshitz [23], we adopt a polarisation tensorial notation  $\rho_{\alpha\beta}$  to characterize quasi-monochromatic plane waves propagating along the  $z$ -axis. This framework is expressed in terms of the three Pauli matrices  $\sigma_1, \sigma_2, \sigma_3$  and the Stokes parameters  $\xi_i$ .

$$(3.1) \quad \begin{aligned} (\rho_{\alpha\beta}) &= \begin{pmatrix} \rho_{xx} & \rho_{xy} \\ \rho_{yx} & \rho_{yy} \end{pmatrix} = \frac{1}{2} \begin{pmatrix} 1 + \xi_3 & \xi_1 - i\xi_2 \\ \xi_1 + i\xi_2 & 1 - \xi_3 \end{pmatrix} \\ &= \frac{1}{2} \left( \mathbb{1}_2 + \sum_{i=1}^3 \xi_i \sigma_i \right), \end{aligned}$$

$$(3.2) \quad \begin{aligned} \xi_1 &= r \sin 2\phi, & \xi_2 &= A, & \xi_3 &= r \cos 2\phi, \\ r &= \sqrt{\xi_1^2 + \xi_3^2}, & \phi &= \frac{1}{2} \arctan \frac{\xi_1}{\xi_3} \end{aligned}$$

The labels  $\alpha, \beta$  run over the coordinates  $(x, y)$  in the plane orthogonal to the  $z$ -axis. In Eq. (3.2) the parameter  $0 \leq r \leq 1$  characterizes the degree of maximal linear polarisation whilst  $-1 \leq A \leq 1$  characterizes the circular polarisation of the beam. Hence, with the notations of Eq. (2.5), the polarisation tensor Eq. (3.1) can be written as:

$$(3.3) \quad (\rho_{\alpha\beta}) = \rho_{r,\phi} + \frac{A}{2} \sigma_2 .$$

The Stokes parameters are related to the (complex) electric field component of the light (Fig. 2).

$$(3.4) \quad \vec{E}(t) = \vec{E}_0(t) e^{i\omega t} = E_x \hat{i} + E_y \hat{j} = (E_\alpha) .$$

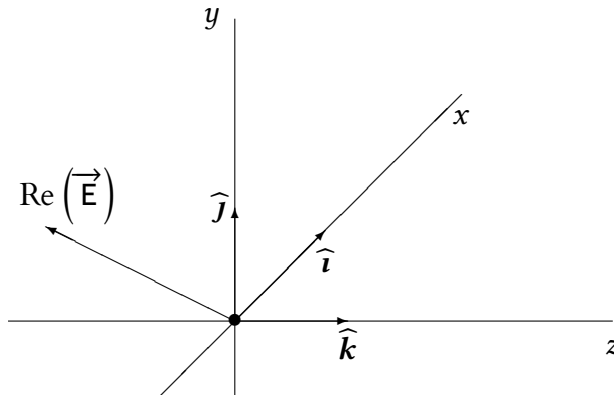


FIGURE 2. A quasi-monochromatic plane wave propagates to the right along the  $z$ -axis. The real part of the electric field lies in the  $x - y$  plane.

The time variation of the electric field  $\vec{E}(t)$  has average frequency  $\omega$ , while its  $\vec{E}_0(t)$  part varies slowly in time. This vector governs the polarisation characteristics of light, which are gauged using Nicol prisms or similar devices. Measurement involves assessing light intensity derived from mean values of quadratic expressions involving field components.

Specifically, these expressions, proportional to  $\mathbf{E}_\alpha \mathbf{E}_\beta$ ,  $\mathbf{E}_\alpha \mathbf{E}_\beta^*$ , and their corresponding complex conjugates, play a crucial role.

Considering  $\mathbf{E}_\alpha \mathbf{E}_\beta = \mathbf{E}_{0\alpha} \mathbf{E}_{0\beta} e^{2i\omega t}$  and  $\mathbf{E}_\alpha^* \mathbf{E}_\beta^* = \mathbf{E}_{0\alpha}^* \mathbf{E}_{0\beta}^* e^{-2i\omega t}$ , it is evident that these expressions feature rapidly oscillating components. Consequently, their temporal averages  $\langle \cdot \rangle_t$  equate to zero.

As a result, the complete characterization of partially polarized light can be succinctly conveyed through the description provided by the tensor components:

$$(3.5) \quad J_{\alpha\beta} := \left\langle \mathbf{E}_{0\alpha} \mathbf{E}_{0\beta}^* \right\rangle_t .$$

The quantity  $J = \sum_\alpha J_{\alpha\alpha} = \langle |\mathbf{E}_{0x}|^2 \rangle_t + \langle |\mathbf{E}_{0y}|^2 \rangle_t$  determines the intensity of the wave, obtained from the measurement of the energy flux transported by the wave. Since this quantity does not concern the properties of polarisation of the wave, one would rather to deal with the normalized Stokes tensor Eq. (3.1), *i.e.*,

$$(3.6) \quad \rho_{\alpha\beta} = \frac{J_{\alpha\beta}}{J} .$$

The light is said completely polarized when the complex amplitude  $\vec{\mathbf{E}}_0$  is time-independent, and so is equal to its time average. Then, the polarisation tensor factorizes as

$$(3.7) \quad (\rho_{\alpha\beta}) = \frac{1}{J} \begin{pmatrix} |\mathbf{E}_{0x}|^2 & \mathbf{E}_{0x} \mathbf{E}_{0y}^* \\ \mathbf{E}_{0x}^* \mathbf{E}_{0y} & |\mathbf{E}_{0y}|^2 \end{pmatrix} = \begin{pmatrix} \mathbf{E}_{0x} / \sqrt{J} \\ \mathbf{E}_{0y} / \sqrt{J} \end{pmatrix} \begin{pmatrix} \mathbf{E}_{0x}^* / \sqrt{J} & \mathbf{E}_{0y}^* / \sqrt{J} \end{pmatrix} ,$$

*i.e.*, is the orthogonal projector along  $\vec{\mathbf{E}}_0$ , and, in quantum terms, a pure state. This case should be put in regard to the other extreme case, namely the non-polarized or natural light, for which all directions in the  $x - y$  plane are equivalent:

$$(3.8) \quad (\rho_{\alpha\beta}) = \frac{1}{2} \delta_{\alpha\beta} .$$

In the general case and with the  $\xi_i$  coordinates introduced in Eq. (3.1),

$$\det(\rho_{\alpha\beta}) = \frac{1}{4} (1 - \xi_1^2 - \xi_2^2 - \xi_3^2) \equiv \frac{1}{4} (1 - P^2),$$

where  $0 \leq P \leq 1$  is called the degree of polarisation, from  $P = 0$  (random polarisation) to  $P = 1$  (total polarisation). Another extreme case holds with circular polarisation. Then  $\vec{E}_0$  is constant and  $E_{0y} = \pm iE_{0x}$ , which gives  $(\rho_{\alpha\beta}) = (1/2)(\mathbb{1}_2 \pm i\sigma_2) = (1/2)(\mathbb{1}_2 \mp \tau_2)$ . As a consequence, the parameter  $-1 \leq A \leq 1$  in Eq. (3.2) is interpreted as the degree of circular polarisation, with  $A = 1$  (resp.  $A = -1$ ) for right (resp. left) circular polarisation, and  $A = 0$  for linear polarisation.

The differentiation between linear and circular polarisations precisely aligns with the decomposition of Eq. (3.1) into its symmetric and anti-symmetric components:

$$(3.9) \quad (\rho_{\alpha\beta}) = \rho_{r,\phi} + \frac{A}{2}\sigma_2 = \frac{1+r}{2}P_\phi + \frac{1-r}{2}P_{\phi+\pi/2} + \frac{A}{2}\sigma_2,$$

with notations of Eq. (2.5). In the present work, we ignore circular polarisation by setting  $A$  to zero. Then the polarisation  $P = r$  and that simplifies the polarisation tensor down to our real density matrix.

#### 4. POLARISATION OF THE LIGHT THROUGH A VON NEUMANN QUANTUM INTERACTION

**4.1. Outcomes of interaction with quantum polariser.** Let us delve into the interaction between a quantum polariser (in the sense given in the introduction) and a partially linear polarised light – an elementary example of a quantum interaction (and, possibly, measurement as well). Our approach is inspired by the example outlined by Peres in [24], but with a specific perspective on two planes and their tensor product. The first plane is the Hilbert space where the states  $\rho_{s,\theta}^P$  of the polariser, treated

as an orientation modifier, are involved. Notably, the action of the rotation generator  $\tau_2 = -i\sigma_2$  on these states corresponds to a rotation of  $\pi/2$ :

$$(4.1) \quad \tau_2 \rho_{s,\theta}^P \tau_2^{-1} = -\tau_2 \rho_{s,\theta}^P \tau_2 = \rho_{s,\theta+\pi/2}^P.$$

The second plane is the Hilbert space on which act the partially linearized polarisation states  $\rho_{r,\phi}^L$  of the plane wave crossing the polariser. Since the exact interaction time is ill-determined, the interaction polariser-light has a time duration interval  $I_M = (t_M - \eta, t_M + \eta)$  centred at  $t_M$ . This interaction is described by the (pseudo-) Hamiltonian operator

$$(4.2) \quad \tilde{H}_{\text{int}}(t) = g_M^\eta(t) \tau_2 \otimes A^L.$$

Here  $g_M^\eta$  has support in  $I_M$  and approximates the Dirac peak as

$$\lim_{\eta \rightarrow 0} \int_{-\infty}^{+\infty} dt f(t) g_M^\eta(t) = f(t_M).$$

The action of the polariser on the light is described by the quantum observable  $A^L$ , *i.e.*, a symmetric matrix, acting on the states of the light. It has the spectral decomposition

$$(4.3) \quad A^L = \lambda_{\parallel} P_\gamma + \lambda_{\perp} P_{\gamma+\pi/2},$$

where the direction defined by  $P_\gamma$  is interpreted as the filter's orientation, while total absorption occurs along the direction  $\gamma + \pi/2$ .

The operator (4.2) is the tensor product of an antisymmetric operator, like the pseudo-Hamiltonian (2.14), for the detector with an operator for the system which is symmetric (*i.e.* Hamiltonian). Nevertheless, the operator  $U(t, t_0)$  defined for  $t_0 < t_M - \eta$  as

$$(4.4) \quad U(t, t_0) = \exp \left[ \int_{t_0}^t dt' g_M^\eta(t') \tau_2 \otimes A^L \right] = \exp [G_M^\eta(t) \tau_2 \otimes A^L],$$

with  $G_M^\eta(t) = \int_{t_0}^t dt' g_M^\eta(t')$ , is an evolution operator. Hence, as soon as  $t > t_M + \eta$ ,  $G_M^\eta(t) = 1$ . From the general formula involving an orthogonal projector  $P$ ,

$$(4.5) \quad \exp(\theta \tau_2 \otimes P) = \mathcal{R}(\theta) \otimes P + \mathbb{1}_2 \otimes (\mathbb{1}_2 - P),$$

we get the expression:

$$(4.6) \quad U(t, t_0) = \mathcal{R}(G_M^\eta(t) \lambda_{||}) \otimes P_\gamma + \mathcal{R}(G_M^\eta(t) \lambda_\perp) \otimes P_{\gamma+\pi/2}.$$

For  $t_0 < t_M - \eta$  and  $t > t_M + \eta$ , we finally obtain for the evolution operator:

$$(4.7) \quad U(t, t_0) = \mathcal{R}(\lambda_{||}) \otimes P_\gamma + \mathcal{R}(\lambda_\perp) \otimes P_{\gamma+\pi/2}.$$

One easily checks that  $U(t, t_0)U(t, t_0)^\dagger = U(t, t_0)^\dagger U(t, t_0) = \mathbb{1}_2 \otimes \mathbb{1}_2$ .

**4.2. Light after interaction.** After having prepared the polariser in the state  $\rho_{s_0, \theta_0}^P$  and its associated observable  $A_L$  acting on the light states, the action of the operator (4.7) on the initial state  $\rho_{s_0, \theta_0}^P \otimes \rho_{r_0, \phi_0}^L$  reads for  $t > t_M + \eta$ :

$$(4.8) \quad \begin{aligned} & U(t, t_0) \rho_{s_0, \theta_0}^P \otimes \rho_{r_0, \phi_0}^L U(t, t_0)^\dagger \\ &= \rho_{s_0, \theta_0 + \lambda_{||}}^P \otimes \frac{1 + r_0 \cos 2(\gamma - \phi_0)}{2} P_\gamma \\ &+ \rho_{s_0, \theta_0 + \lambda_\perp}^P \otimes \frac{1 - r_0 \cos 2(\gamma - \phi_0)}{2} P_{\gamma+\pi/2} \\ &+ \frac{1}{4} (\mathcal{R}(\lambda_{||} - \lambda_\perp) + s_0 \sigma_{2\theta_0+1}) \otimes r_0 \sin 2(\gamma - \phi_0) P_\gamma \tau_2 \\ &- \frac{1}{4} (\mathcal{R}(\lambda_\perp - \lambda_{||}) + s_0 \sigma_{2\theta_0+1}) \otimes r_0 \sin 2(\gamma - \phi_0) \tau_2 P_\gamma. \end{aligned}$$

As expected from the standard theory of quantum measurement, this formula indicates that the probability for the observable  $A^L$  to orientate

along  $\gamma$  is given by the Born rule:

$$(4.9) \quad \begin{aligned} & \text{Tr} \left[ \left( U(t, t_0) \rho_{s_0, \theta_0}^P \otimes \rho_{r_0, \phi_0}^L U(t, t_0)^\dagger \right) (\mathbb{1} \otimes P_\gamma) \right] \\ &= \text{Tr} \left[ \rho_{r_0, \phi_0}^L P_\gamma \right] = \frac{1 + r_0 \cos 2(\gamma - \phi_0)}{2} = \frac{1 - r_0}{2} + r_0 \cos^2(\gamma - \phi_0), \end{aligned}$$

whereas its probability to orientate along  $\gamma + \pi/2$  is:

$$(4.10) \quad \begin{aligned} & \text{Tr} \left[ \left( U(t, t_0) \rho_{s_0, \theta_0}^P \otimes \rho_{r_0, \phi_0}^L U(t, t_0)^\dagger \right) (\mathbb{1} \otimes P_{\gamma+\pi/2}) \right] \\ &= \text{Tr} \left[ \rho_{r_0, \phi_0}^L P_{\gamma+\pi/2} \right] = \frac{1 - r_0 \cos 2(\gamma - \phi_0)}{2} = \frac{1 - r_0}{2} + r_0 \sin^2(\gamma - \phi_0), \end{aligned}$$

For the completely linear polarisation of the light, i.e.  $r_0 = 1$ , we recover the familiar Malus laws,  $\cos^2(\gamma - \phi_0)$  and  $\sin^2(\gamma - \phi_0)$  respectively. Hence, after the interaction between polariser–partially linear polarised light, the polarisation of the light is described by the new density matrix, obtained by tracing out the polariser part in Eq. (4.8),

$$(4.11) \quad \rho_{r', \phi'}^L = \text{Tr}_M \left[ U(t, t_0) \rho_{s_0, \theta_0}^P \otimes \rho_{r_0, \phi_0}^L U(t, t_0)^\dagger \right] = \frac{1 + r'}{2} P_{\phi'} + \frac{1 - r'}{2} P_{\phi'+\pi/2}.$$

Details of calculations of the parameters  $r'$  and  $\phi'$  are given in Appendix A. We obtain:

$$(4.12)$$

$$r' = r_0 \sqrt{a^2 + b^2} = r_0 \sqrt{\cos^2 2(\gamma - \phi_0) + \cos^2(\lambda_{\parallel} - \lambda_{\perp}) \sin^2 2(\gamma - \phi_0)} \leq r_0,$$

$$(4.13)$$

$$\tan \phi' = \frac{\sqrt{a^2 + b^2} - a}{b}, \quad b \neq 0, \Leftrightarrow \tan 2\phi' = \frac{b}{a},$$

where

$$(4.14) \quad a = \cos 2(\gamma - \phi_0) \cos 2\gamma + \cos(\lambda_{\parallel} - \lambda_{\perp}) \sin 2(\gamma - \phi_0) \sin 2\gamma,$$

$$(4.15) \quad b = \cos 2(\gamma - \phi_0) \sin 2\gamma - \cos(\lambda_{\parallel} - \lambda_{\perp}) \sin 2(\gamma - \phi_0) \cos 2\gamma.$$

From these expressions, one observes that the initial state  $\rho_{r_0, \phi_0}^L$  of the light is not modified if  $\gamma = \phi_0$ . Although the initial state  $\rho_{s_0, \theta_0}^P$  of the polariser serves as an ancilla necessary for implementing the action  $A^L$  of the polariser on the light, its own state is altered by the interaction, as detailed in Appendix B. Additionally, in the Appendix C, we explore the case of the infinitesimal evolution following the interaction in relation with the GLKS dynamical system.

In order to physically represent the rôle of the polariser as forcing the light to be partially polarised along its eigendirection  $\gamma$ , the angle  $\phi'$  of the light state after the action of the polariser must be the same as  $\gamma$ . From this constraint and from Eq. (4.13) we obtain

$$(4.16) \quad \tan 2\phi' = \frac{\tan 2\gamma - \cos(\lambda_{\parallel} - \lambda_{\perp}) \tan 2(\gamma - \phi_0)}{1 + \cos(\lambda_{\parallel} - \lambda_{\perp}) \tan 2(\gamma - \phi_0) \tan 2\gamma} = \tan 2\gamma,$$

which holds if  $\lambda_{\parallel} - \lambda_{\perp} = (2k + 1)\frac{\pi}{2}$ . It follows for the parameter  $r'$  the attenuation:

$$(4.17) \quad r' = r_0 \sqrt{\cos^2 2(\gamma - \phi_0) + \cos^2(\lambda_{\parallel} - \lambda_{\perp}) \sin^2 2(\gamma - \phi_0)} = r_0 |\cos 2(\gamma - \phi_0)|,$$

which gives the Malus law:

$$(4.18) \quad \frac{1 + r'}{2} = \frac{1 - r_0}{2} + r_0 \cos^2(\gamma - \phi_0) \quad \text{for} \quad \gamma \leq \phi_0 + \frac{\pi}{2}.$$

## 5. CLASSICAL POLARISATION OF THE LIGHT VERSUS QUANTUM FORMALISM

In the previous section, we discussed the interaction between what we refer to as a quantum polarizer and light, treating it as a unitary process. This approach allows us to calculate the probability of observing each eigenvalue or eigendirection, as expressed in Eq. (4.3), while deliberately ignoring the inherent irreversibility associated with any realistic quantum measurement – namely, the reduction to an eigenstate of the

observable being measured. During such a classical process, it is expected that the polariser enforces one of its eigendirections from Eq. (4.3) onto the light, say  $\gamma$ , as previously discussed. Consequently, we should explore the possibility of a collapse where  $\phi' = \gamma$  in Eq. (4.13), either through a projection-valued measure or, in a more sophisticated analysis, through a positive-operator-valued measure. We will now delve deeper into what is generally understood by classical polarization and explore the potential connections with the content presented in Section 4.

A polarisation element is an essential optical device used to precisely control and manipulate the polarisation state of light [25]. The primary function of a polarisation element is to transform light between different polarisation states. Polarisers and retarders are the most commonly used and effective polarisation elements in the field of optics. In this context, polarisation properties can be classified into three groups, which are depolarisation, diattenuation, and retardance. Depolarisation can be described as a random reduction in the degree of polarisation, while diattenuation is an alteration in amplitude that depends on polarisation. Retardance is a modification of the phase related to a specific polarisation. In our work, we focus on the diattenuation effect to characterize our real polariser and establish the connection between our quantum approach to polarisation with these (classical) polarisation properties. We recall that a polariser is an optical element that transmits light into a desired polarisation state, independent of the incident state. An important aspect of the polariser is that the transmitted orthogonal polarised state is approximately zero for the real polariser and exactly zero for the ideal polariser. Thus, we can define the following ratio for the diattenuation

present in a polariser

$$(5.1) \quad D = \frac{T_{max} - T_{min}}{T_{max} + T_{min}},$$

where  $T_{max}$  is the maximal transmittance when compared among all polarisation states, and  $T_{min}$  is the minimum transmittance. The ideal polariser has  $D = 1$ . On the other hand  $D = 0$  represents a device without interaction or one that transmits all the polarisation states in the same way. One can recognize the transmittance as the result presented at Eq. (4.11), and the respective maximum and minimal values are

$$(5.2) \quad T_{max} = \frac{1 + r'}{2}, \quad \phi' = \gamma,$$

$$(5.3) \quad T_{min} = \frac{1 - r'}{2}, \quad \phi' = \gamma + \frac{\pi}{2}.$$

Therefore, in this context, due to the normalization of the states by the intensity of the light as described in Eq. (3.7), the diattenuation  $D$  is equivalent to the degree of depolarisation  $r'$ . It results that the so-called extinction ratio is given in our case by:

$$(5.4) \quad \epsilon_r = \frac{1 + D}{1 - D} = \frac{1 + r'}{1 - r'}.$$

## 6. GENERAL SETTING FOR QUANTUM CIRCUITS IN THE PLANE

**6.1. GKLS equations.** The purpose of the present work is to adapt the study of complexity of quantum circuit to the material described in the previous sections. Firstly, we aim to deal with quantum states  $\rho_{r,\phi}$  and not just pure states, and, secondly, to consider such states as standing for open systems, which means that their parameters  $r$  and  $\phi$  evolve according to the dynamical system described by Eqs. (2.19) and (2.20). We exclude the case  $\beta = 0$  since it implies  $\alpha = 0$  and just describes the unitary evolution  $\phi(t) = \phi_0 \exp \left[ - \int_{t_0}^t dt' \mathcal{E}(t') \right]$ .

In the scope of this paper, we also deviate from the conventional GKLS equations by broadening their application to encompass evolution models with time-dependent coefficients. As regards of this extension and on a more formal level [18, 26, 27], one describes the evolution of density operators in the space  $\mathcal{B}(\mathcal{H})$  of bounded operators on the Hilbert space  $\mathcal{H}$  in terms of completely positive trace-preserving (CPTP) (dynamical) maps:

(6.1)

$$\Lambda_{t,t_0} : \mathcal{B}(\mathcal{H}) \mapsto \mathcal{B}(\mathcal{H}), \quad \Lambda_{t,t_0} \rho_0 = \text{Tr}_E \left( U(t, t_0) \rho_0 \otimes \rho_E U^\dagger(t, t_0) \right),$$

where  $\Lambda_{t,t_0}$  obeys the time-local but inhomogeneous master equation  $\partial_t \Lambda_{t,t_0} = \mathcal{L}_t \circ \Lambda_{t,t_0}$ . The density operator  $\rho_0$  represents the system's state at the initial time  $t_0$ , while  $\rho_E$  corresponds to the state of the environment. This  $\Lambda_{t,t_0}$  is CPTP iff  $\mathcal{L}_t$  is of the GLKS form for all  $t$ , *i.e.*, is inhomogeneous generalization of a semigroup evolution. In our case this means that the parameters  $\alpha$  and  $\beta$  are time-dependent. Hence we will also deal with the time-inhomogeneous Lindblad system:

$$(6.2) \quad \dot{\phi} = \alpha(t) \sin 4\phi - \mathcal{E}(t),$$

$$(6.3) \quad \frac{\dot{r}}{r} = -2\alpha(t) \cos 4\phi - \beta(t).$$

Like for Eq. (2.21), Eq. (6.3) is easily integrable once given a solution  $\phi(t)$  to Eq. (6.2):

$$(6.4) \quad r(t) = r_0 \exp \left[ - \int_{t_0}^t (2\alpha(t') \cos 4\phi(t') + \beta(t')) dt' \right].$$

**6.2. Metric structure of mixed states for the Euclidean plane.** Concerning the family  $\{\rho_{r,\phi}, 0 \leq r \leq 1, \phi \in [0, \pi)\}$  of density matrices we are dealing with, it is important for the sequel to describe the metric structure to which they pertain.

Any density operator  $\rho$  has unit trace norm,  $\|\rho\| = \text{tr}\sqrt{\rho\rho^\dagger} = \text{tr}\sqrt{\rho^2} = 1$ . This property is essential in defining the *trace distance* between quantum states:

$$(6.5) \quad d_{\text{TN}}(\rho_{r,\phi}, \rho_{r',\phi'}) = \frac{1}{2} \text{tr} \sqrt{(\rho_{r,\phi} - \rho_{r',\phi'})^\dagger (\rho_{r,\phi} - \rho_{r',\phi'})} = \frac{1}{2} \sum_{i=1}^2 |\lambda_i|,$$

where  $\lambda_i$  is the  $i$ -th eigenvalue of the the matrix  $(\rho_{r,\phi} - \rho_{r',\phi'})$ . It is easy to show that

$$(6.6) \quad d_{\text{TN}}(\rho_{r,\phi}, \rho_{r',\phi'}) = \frac{1}{2} \sqrt{r^2 + r'^2 - 2rr' \cos(2\phi - 2\phi')} = \frac{1}{2} \|(r, 2\phi) - (r', 2\phi')\|,$$

i.e., is one-half of the Euclidean distance between the points  $(r, 2\phi)$  and  $(r', 2\phi')$ . Note that for  $r = r'$  this expression simplifies to

$$(6.7) \quad d_{\text{TN}}(\rho_{r,\phi}, \rho_{r,\phi'}) = r |\sin(\phi - \phi')|.$$

Geodesic curves corresponding to this metric are found as the solution of the the Euler-Lagrange equations:

$$(6.8) \quad \ddot{\phi}(t) + 2 \frac{\dot{r}(t)}{r(t)} \dot{\phi}(t) = 0, \quad \frac{\ddot{r}(t)}{r(t)} - \dot{\phi}^2(t) = 0.$$

As one might expect, they are straight lines and are described in polar coordinates by:

$$(6.9) \quad r = \frac{1}{C_3 \cos \phi + C_4 \sin \phi},$$

where the coefficients can be obtained via the chosen reference and target states

$$(6.10) \quad C_3 = \frac{r_T \sin \phi_T - r_R \sin \phi_R}{r_T r_R \sin(\phi_T - \phi_R)}, \quad C_4 = \frac{-r_T \cos \phi_T + r_R \cos \phi_R}{r_T r_R \sin(\phi_T - \phi_R)},$$

Note that one can rewrite the trace distance  $d_{\text{TN}}$  using the Stokes parameters presented in Eq. (3.2)

$$(6.11) \quad d_{\text{TN}}(\rho_{r,\phi}, \rho_{r',\phi'}) = \frac{1}{2} \sqrt{(\xi_1 - \xi'_1)^2 + (\xi_3 - \xi'_3)^2},$$

where  $\xi_1^2 + \xi_3^2 \leq 1$ , and  $0 \leq d_{\text{TN}} \leq 1$ .

## 7. SOME ANALYTIC SOLUTIONS TO GKLS EQUATIONS

We exhibit some analytic solutions for the dynamical system described by Eqs. (2.19) and (2.20) describing the time-homogeneous case (constant coefficients), and Eqs. (6.2)–(6.3) for inhomogeneous configuration. We first explore specific cases of the homogeneous GLKS equations for which the energy  $\mathcal{E}$  is constant, and then for which the angular velocity  $\dot{\phi}$  is constant. Second we study the time-inhomogeneous case when  $\phi$  is constant.

**7.1. Constant energy  $\mathcal{E}$ .** The equations (2.19) and (2.20) have constant coefficients  $\alpha$  and  $\beta$ . Let us consider the energy parameter  $\mathcal{E}$  in Eq. (2.19) as constant. Integrating the system yields:

$$(7.1) \quad \int_{\phi(t_0)}^{\phi(t)} \frac{d\phi'}{\alpha \sin 4\phi' - \mathcal{E}} = t - t_0,$$

The general form of this integral is found in [28], 2.55.1.3:

$$(7.2) \quad \int \frac{dx}{a + b \sin x} = \frac{2}{\sqrt{a^2 - b^2}} \arctan \left[ \frac{a \tan \frac{x}{2} + b}{\sqrt{a^2 - b^2}} \right] \quad \text{if } a^2 > b^2,$$

$$(7.3) \quad \frac{1}{\sqrt{b^2 - a^2}} \ln \left[ \frac{a \tan \frac{x}{2} + b - \sqrt{b^2 - a^2}}{a \tan \frac{x}{2} + b + \sqrt{b^2 - a^2}} \right] \quad \text{if } a^2 < b^2.$$

*Case  $\mathcal{E}^2 > \alpha^2$ .* The application of Eq. (7.2) to Eq. (7.1) gives the solution:

$$(7.4) \quad \phi(t) = \frac{1}{2} \arctan \left[ \frac{-\omega_1}{\mathcal{E}} \tan(2\omega_1 \Delta t + c_0) + \frac{\alpha}{\mathcal{E}} \right] + \frac{n\pi}{2},$$

where

$$(7.5) \quad \Delta t = t - t_0, \quad \omega_1 = \sqrt{\mathcal{E}^2 - \alpha^2}, \quad c_0 = \arctan \left[ \frac{-\mathcal{E} \tan 2\phi(t_0) + \alpha}{\omega_1} \right].$$

Here  $n \in \mathbb{Z}$  must be carefully chosen to insure the continuity of  $\phi(t)$  in the interval  $[0, \pi)$ . In Fig. 3, we plot the trajectory of the density matrix in the upper half-unit disk, where  $\mathbf{r}(t) = (r(t) \cos \phi(t), r(t) \sin \phi(t))$  for two representative cases. The  $r(t)$  values were obtained via numerical integration of the  $\cos 4\phi(t)$  in Eqs. (2.21) or (6.4) for constant  $\beta$ . In this context, it becomes evident that making the parameter values vary leads to disparate trajectories, whether exhibiting cyclic patterns or not, across the upper half-unit disk. This connection becomes explicit when one identifies the constant  $\omega_1$  with an angular frequency. Then, the period  $T$  of the  $\phi$  cycle is  $T = \pi/(2\omega_1)$ , where  $\pi$  is the periodicity of the tangent function.

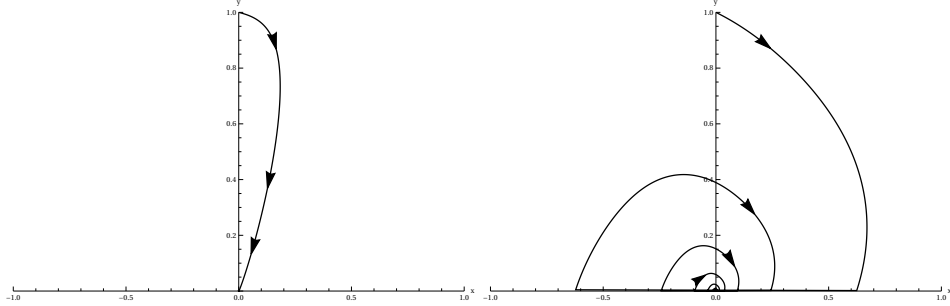


FIGURE 3. Plot of the trajectory of the density matrix with initial conditions  $r(0) = 1$  and  $\phi(0) = \pi/2$ . Both figures have the energy  $\mathcal{E} = 10$ , but different parameters  $\alpha = -9$ ,  $\beta = 20$  (left),  $\alpha = 0.5$ , and  $\beta = 3$  (right).

*Case  $\mathcal{E}^2 < \alpha^2$ .* Eq. (7.1) now leads to the solution:

$$(7.6) \quad \phi(t) = \frac{1}{2} \arctan \left[ \frac{\alpha}{\mathcal{E}} + \frac{\gamma}{\mathcal{E}} \coth(2\gamma\Delta t + c_2) \right] + \frac{n\pi}{2},$$

where we have introduced

$$(7.7) \quad \gamma = \sqrt{\alpha^2 - \mathcal{E}^2}, \quad c_2 = \frac{1}{2} \ln \left[ \frac{-\mathcal{E} \tan 2\phi(0) + \alpha - \gamma}{-\mathcal{E} \tan 2\phi(0) + \alpha + \gamma} \right].$$

The integer  $n$  is responsible for the continuity of  $\phi(t)$  in the upper half-unit disk. The parameter  $\gamma$  can be viewed as an attenuation constant for the variable  $\phi$ , given the behavior of the coth function, which tends towards unity for extended time intervals.

**7.2. Constant angle  $\phi$ .** Considering Eqs. (2.19)–(2.20) of the inhomogeneous GLKS system, we analyze the case where  $\dot{\phi} = 0$ . Then, the  $\phi$  variable does not change over time, and this implies

$$(7.8) \quad \mathcal{E}(t) = \alpha(t) \sin 4\phi_R,$$

where  $\phi_R$  is the initial condition for  $\phi$ . We have now to deal with the inhomogeneous GLKS case. Then the radial function reads:

$$(7.9) \quad r(t) = r_R \exp \left[ - \int_0^t (2\alpha(t') \cos 4\phi_R + \beta(t')) dt' \right],$$

where  $r_R = r(t_0)$  is the reference state  $r$  value. This integrand decreases over time, because  $2\alpha(t) \cos 4\phi_R + \beta(t) = h_1(t)(1 + \cos 4\phi_R) + h_2(t)(1 - \cos 4\phi_R) > 0$  for  $h_1(t)$  and  $h_2(t)$  being positive. As a consequence, the trajectory in the upper half disk forms a straight line leading to the origin, as illustrated in Fig. 4, irrespective of whether the parameters are constant or time-dependent. A special situation happens when  $2\alpha(t) \cos 4\phi_R + \beta(t) = 0$ . This leads to  $r(t) = r_R$ , the circuit trajectory thus collapses to a single fixed point.

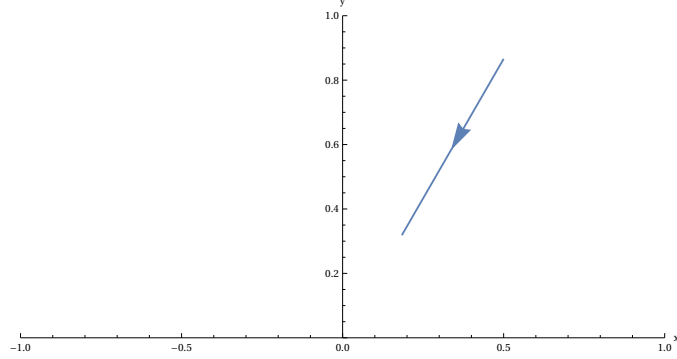


FIGURE 4. Straight line trajectory that obeys Eq. (7.8) with  $\phi_R = \pi/3$ ,  $r_R = 1$ ,  $\alpha = 1$ , and  $\beta = 2$ .

**7.3. Constant  $\dot{\phi}$ .** When  $\alpha = 0$  and both  $\beta$  and  $\mathcal{E}$  are constant, Eqs. (2.19) and (2.20) become  $\dot{\phi} = -\mathcal{E}$  and  $\dot{r} = -\beta$ , respectively. The two equations are simply solved through  $\phi(t) = \phi_R - \mathcal{E}\Delta t$  and  $r = r_R e^{-\beta\Delta t}$ . Therefore, within the quantum circuit framework, for which  $t_R$  and  $t_T$  are references and target times respectively, one can directly determine the values of the system parameters in function of the reference and target states variables:

$$(7.10) \quad \mathcal{E} = \frac{\phi_R - \phi_T}{t_T - t_R}, \quad \beta = \frac{1}{t_T - t_R} \ln \frac{r_R}{r_T}.$$

Note that  $\phi$  is restricted to the upper half-plane,  $\phi \in [0, \pi)$  and so the solution is  $\pi$  cyclic.

## 8. NUMERICAL APPROACH TO COMPLEXITY CIRCUIT

We now enter into the heart of our project in dealing with sequences of  $N$  gates (e.g., quantum polarisers) through the path followed by the state  $\rho_{r,\phi}^L$  from the referent  $\rho_{r_R, \phi_R}^L$  to the target  $\rho_{r_T, \phi_T}^L$ . Our objective is to ensure that the states closely follow the geodesics associated with the trace distance metric (6.5), based on the reasonable assumption that these

geodesics represent the optimal circuits. Specifically, we aim to approximate the geodesics in Eq. (6.9) using a sequence of trajectories, each with constant parameters. This condition arises from the fact that such trajectories are the easiest to implement in dealing with the GLKS dynamics.

Precisely, the curve initiates from the reference state  $\rho^L(r_R, \phi_R)$  and ends at a target state  $\rho^L(r_T, \phi_T)$ . Assuming that the environment interacts with the state, our system is viewed as an open system whose evolution is determined by the GKLS equation (Subsubsec. 2.3.2). We consider an isotropic environment, where the decay rates are constant  $h_1 = h_3 = 1$ , i.e.,  $\alpha = 0$  and  $\beta = 2$ . Moreover we choose a constant pseudo-Hamiltonian with  $\mathcal{E} = -2$ . Without the action of a quantum polariser, the system evolves according to the GKLS equations, and it naturally changes its state in the sense of depolarisation. We then impose the action of a sequence of quantum polarisers (gates) in order to force the light state to adhere closely to the geodesic. Both the geodesic and the trajectory with constant  $\mathcal{E}, \beta, \alpha$  have  $\dot{r} < 0$ . Along these lines, we know that  $r(t)$ , as a monotonically decreasing function, is one-to-one. Then, rather than calculating the distance from the trajectory to the geodesic at each moment, we compare the geodesic state with the time-evolving state at the same radial coordinate  $r$ . It results the simplified expression for the trace distance Eq. (6.7):

$$(8.1) \quad d_{\text{geo}} \left( \rho_{r,\phi}^L, \rho_{r,\phi_{\text{geo}}}^L \right) = r |\sin(\phi - \phi_{\text{geo}})|,$$

where  $\phi_{\text{geo}}$  is the angle parameter of the geodesic state. We want to identify the minimum number of gates necessary to maintain the constant parameter path within a defined accuracy (or tolerance) threshold  $\epsilon$

$$(8.2) \quad d_{\text{geo}} \left( \rho_{r,\phi}^L, \rho_{r,\phi_{\text{geo}}}^L \right) \leq \epsilon.$$

Whenever the state  $\rho_{r,\phi}^L$  deviates from  $\rho_{r,\phi_{\text{geo}}}^L$  by more than  $\epsilon$ , we implement the action of a quantum polariser with an angle  $\gamma = \phi_{\text{geo}}$  to bring the state back close to the geodesic. Essentially, this strategy involves applying the quantum polariser's action  $A^L$  whenever the state deviates from the geodesic by more than the maximum distance defined in Eq. (8.2). To demonstrate the application of this strategy, we select several representative cases, as defined in Table 1, and illustrate them in Fig. 5.

The values of the parameters of the target and reference states are the ones given in the example (a) of Table 1. We choose an accuracy of  $\epsilon = 0.05$ . Whenever the trace distance outstretches the accuracy we employ the polariser to put the state at the same angle as the geodesic.

Example	$\phi_R$	$r_R$	$\phi_T$	$r_T$
a	0	1	$\pi/6$	0.5
b	$\pi/3$	1	$\pi/2$	0.5
c	$\pi/4$	1	$\pi/12$	0.5
d	$11\pi/12$	1	$3\pi/4$	0.5

TABLE 1. Our selected values for the reference state variables  $\phi_R$ ,  $r_R$  (all are for pure states), and the target state variables  $\phi_T$ ,  $r_T$ .

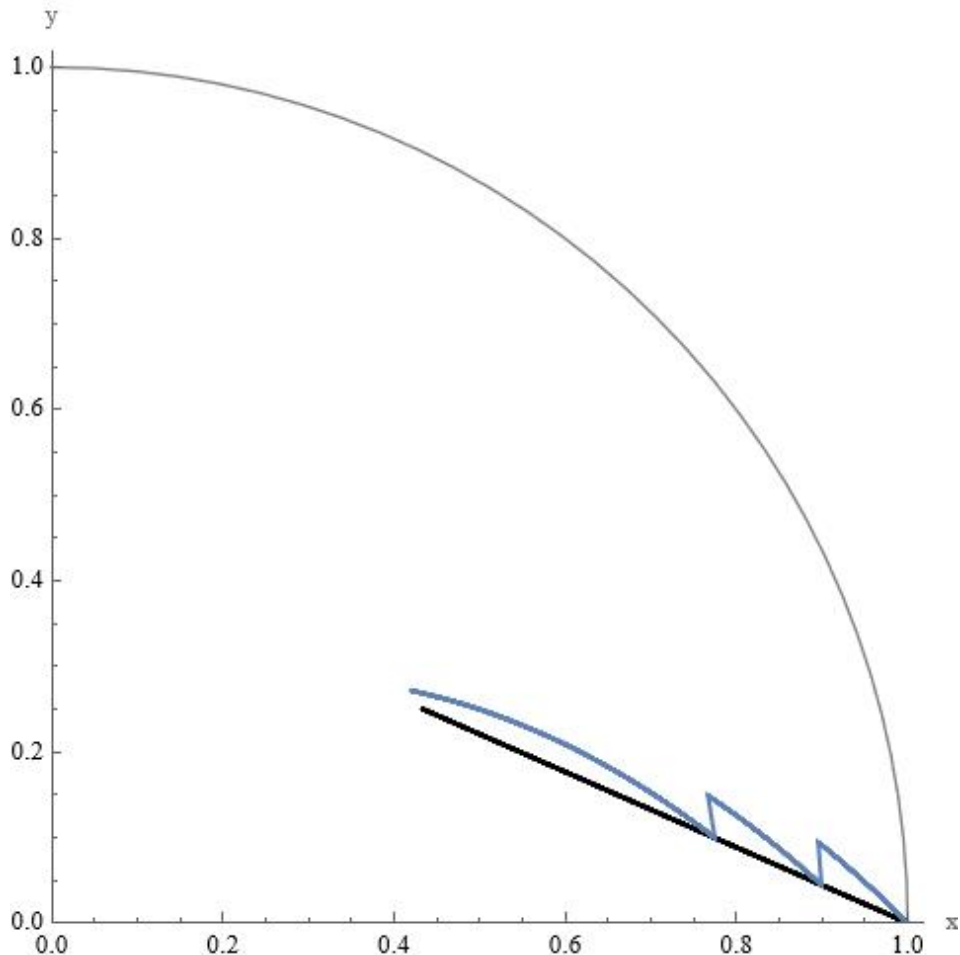


FIGURE 5. The black line represents the geodesic related to the trace distance and for example (a) of the table 1, and the blue curves represent the trajectory of the quantum state evolved accordingly with GLKS equations. When the distance reaches a chosen accuracy  $\epsilon = 0.05$ , we place a quantum polariser to change the angle of the polarisation to be the same as the one at the geodesics. The action of the polarization can be viewed as the abruptly change in the quantum state path.

To analyze the complexity of this quantum circuit, we apply the same procedure to all the examples listed in Table 1. By varying the accuracy parameter, we determine the corresponding number of gates required. The results are presented in the Log-Log plot in Fig. 6, along with a linear fit to the data.

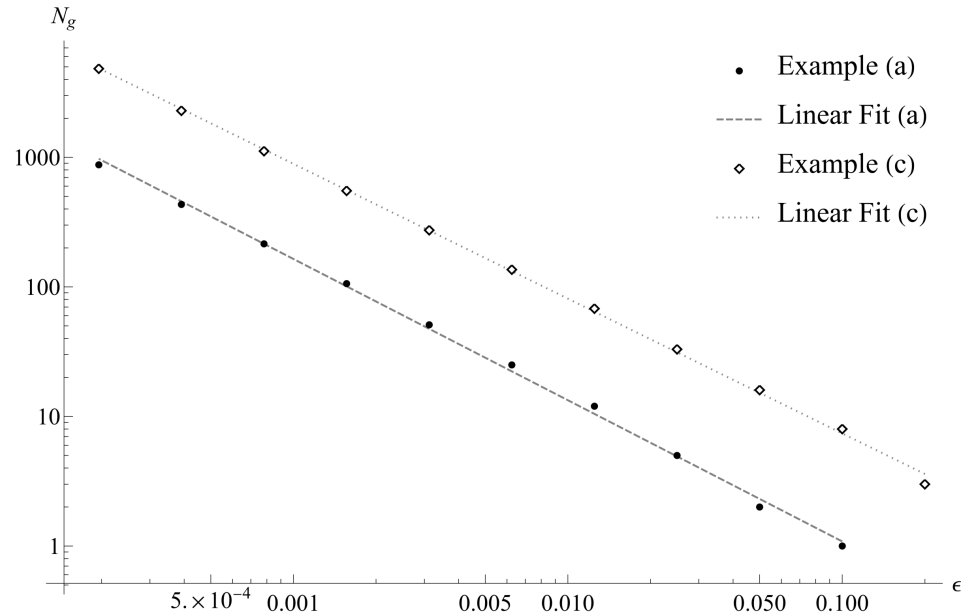


FIGURE 6. The Log-Log plot of the number of polarisers for each accuracy related to examples (a) and (c) of the table 1. The metric here is defined by the trace distance. The pairs of examples (a) and (b), and (c) and (d) have the same data. Therefore, they share the same results for the estimates of the linear fit: (a)  $m = -1.05469$ ,  $n = -1.09012$ , (c)  $m = -0.171026$ ,  $n = -1.04029$ . The examples (b) and (d) are omitted in the figure.

It can be observed that, for examples (a) and (b) in Table 1, the same number of gates is needed to keep the path close to the geodesics, regardless of the accuracy parameter. Similarly, examples (c) and (d) exhibit analogous behavior. The distinction between the pairs of examples (a,b) and (c,d) arises from the variation of  $\phi$  in the geodesics compared to the constant parameter path. Specifically, in examples (a) and (b), both the geodesics and the trajectories described by the GKLS equations have  $\dot{\phi} > 0$ , whereas in examples (c) and (d), the geodesics have  $\dot{\phi} < 0$ .

From the linear fit parameters in  $\log N_g = m + n \log \epsilon$ , we observe that in both cases (a,b) and (c,d) the circuits follow a power law:

$$(8.3) \quad N_g \approx 10^{-1.05} \times \epsilon^{-1.09} \quad \text{examples (a, b),}$$

$$(8.4) \quad N_g \approx 10^{-0.17} \times \epsilon^{-1.04} \quad \text{examples (c, d).}$$

These power-law behaviors are consistent with the typical patterns observed in efficient algorithms, avoiding the exponential growth commonly associated with increased complexity. We regard these findings as the most significant insights from our exploration of this simple model of an open quantum circuit.

## 9. CONCLUSION

We have developed a quantum framework for the Euclidean plane, offering a detailed overview of the fundamental elements necessary for its representation. This framework incorporates the use of Dirac notation to describe the Euclidean plane, defines both pure and mixed states, and clarifies the role of quantum observables. We further demonstrate how this formalism can be interpreted through the lens of linear polarisation variation of light interacting with a concept we define as a quantum polariser. Additionally, we explore the time evolution of both closed and

open quantum systems, with the latter being governed by the GKLS (Lindblad) equation, which we reformulate as a dynamical system.

In this context, we have presented analytic solutions for the dynamical system resulting from the homogeneous GKLS equation with constant energy and constant angular velocity  $\dot{\phi}$ , and specific cases for the non-homogeneous GKLS equation with constant angle  $\phi$ . With the help of those constant parameter solutions, we have investigated the number of gates  $N_g$  requested to suitably approximate the geodesic. In other words, for an open quantum system, where states are represented as points on the upper half of the unit disk, we addressed the problem of achieving a target mixed state  $\rho_T$  from a reference (generally pure) state  $\rho_R$  by attempting to follow as closely as possible, a geodesic determined by the trace distance metric. Such a geodesic the latter is naturally considered as an optimal circuit.

We have proposed a strategy to determine  $N_g$  for a given geometric configuration and desired accuracy. Notably, we observed that the minimum number of gates  $N_g$  follows a power-law scaling with respect to the accuracy, while keeping the maximum allowed distance constant. This behavior aligns with patterns commonly seen in efficient algorithms, effectively avoiding exponential growth.

It is crucial to highlight the broad applicability of this strategy, as it can be implemented with alternative definitions of distance. This concept can be extended to closed or open systems featuring one or more qubits, and, of course, systems that are described by quantum mechanics with complex numbers, like spin 1/2 systems, two level atoms, and beyond. Other potential applications of the present approach include addressing time optimality questions in quantum evolution, as explored in works such as [29, 30]. Additionally, this approach could contribute to

the rapidly advancing field of quantum thermodynamics; relevant examples in this context can be found in [31, 32].

**APPENDIX A. DENSITY MATRIX FOR LIGHT AFTER POLARISATION  
INTERACTION**

We here give the details of the calculations of the parameters  $r'$  and  $\phi'$  in Eq. (4.11). With the notations

$$A^L = \lambda_{\parallel} P_{\gamma} + \lambda_{\perp} P_{\gamma+\pi/2},$$

$$\delta = \lambda_{\parallel} - \lambda_{\perp},$$

$$\zeta = 2(\gamma - \phi_0),$$

and from the expression Eq. (4.8), we successively have:

$$\begin{aligned} \rho_{r',\phi'}^L &= \text{Tr}_M \left[ U(t, t_0) \rho_{s_0, \theta_0}^M \otimes \rho_{r_0, \phi_0}^L U(t, t_0)^\dagger \right] \\ &= \frac{1 + r_0 \cos \zeta}{2} P_{\gamma} + \frac{1 - r_0 \cos \zeta}{2} P_{\gamma+\pi/2} + \frac{r_0}{2} \cos \delta \sin \zeta [P_{\gamma}, \tau_2] \\ &= \frac{1}{2} + \frac{r_0}{2} \begin{pmatrix} \cos \zeta & \cos \delta \sin \zeta \\ -\cos \delta \sin \zeta & \cos \zeta \end{pmatrix} \sigma_{2\gamma} \equiv \frac{1}{2} + \frac{r_0}{2} \begin{pmatrix} a & b \\ b & -a \end{pmatrix}, \end{aligned}$$

with

$$a = \cos \zeta \cos 2\gamma + \cos \delta \sin \zeta \sin 2\gamma,$$

$$b = \cos \zeta \sin 2\gamma - \cos \delta \sin \zeta \cos 2\gamma.$$

The spectral decomposition of the matrix  $\begin{pmatrix} a & b \\ b & -a \end{pmatrix}$  reads as

$$\begin{pmatrix} a & b \\ b & -a \end{pmatrix} = \sqrt{a^2 + b^2} (P_{\varepsilon} - P_{\varepsilon+\pi/2}) = \sqrt{a^2 + b^2} \sigma_{2\varepsilon},$$

with

$$\tan \varepsilon = \frac{\sqrt{a^2 + b^2} - a}{b}, \quad b \neq 0.$$

Thus, by identification with  $\rho_{r',\phi'}^L = \frac{1+r'}{2} P_{\phi'} + \frac{1-r'}{2} P_{\phi'+\pi/2}$  we find:

$$r' = r_0 \sqrt{a^2 + b^2} = r_0 \sqrt{\cos^2 \zeta + \cos^2 \delta \sin^2 \zeta} \leq r_0, \quad \phi' = \varepsilon.$$

## APPENDIX B. QUANTUM POLARISER AFTER INTERACTION

It is interesting to see what the state of the quantum polariser becomes after interaction:

(B.1)

$$\rho_{s',\theta'}^P = \text{Tr}_L \left[ U(t, t_0) \rho_{s_0,\theta_0}^P \otimes \rho_{r_0,\phi_0}^L U(t, t_0)^\dagger \right] = \frac{1+s'}{2} P_{\theta'} + \frac{1-s'}{2} P_{\theta'+\pi/2}.$$

First we obtain the convex combination of two states:

$$(B.2) \quad \rho_{s',\theta'}^P = \frac{1+r_0 \cos 2(\gamma - \phi_0)}{2} \rho_{s_0,\theta_0+\lambda_{\parallel}}^P + \frac{1-r_0 \cos 2(\gamma - \phi_0)}{2} \rho_{s_0,\theta_0+\lambda_{\perp}}^P.$$

Then, we easily obtain  $s'$  and  $\theta'$  from the general convex superposition formula:

$$(B.3) \quad \begin{aligned} \lambda_1 \rho_{r_1,\phi_1} + \lambda_2 \rho_{r_2,\phi_2} &= \rho_{r,\phi}, \quad \lambda_1 + \lambda_2 = 1, \quad \lambda_1, \lambda_2 \geq 0, \\ r &= \sqrt{\lambda_1^2 r_1^2 + \lambda_2^2 r_2^2 - 2\lambda_1\lambda_2 r_1 r_2 \cos 2(\phi_1 - \phi_2)} \\ e^{2i\phi} &= \frac{\lambda_1 r_1 e^{2i\phi_1} + \lambda_2 r_2 e^{2i\phi_2}}{\sqrt{\lambda_1^2 r_1^2 + \lambda_2^2 r_2^2 - 2\lambda_1\lambda_2 r_1 r_2 \cos 2(\phi_1 - \phi_2)}}. \end{aligned}$$

Applied to the case Eq. (B.2) we obtain:

(B.4)

$$\begin{aligned} s' &= \frac{s_0}{\sqrt{2}} \sqrt{\left(1+r_0^2 \cos^2 2(\gamma - \phi_0)\right) - \left(1-r_0^2 \cos^2 2(\gamma - \phi_0)\right) \cos 2(\lambda_{\parallel} - \lambda_{\perp})}, \\ e^{2i\theta'} &= \sqrt{2} e^{2i\theta_0} \frac{(1+r_0 \cos 2(\gamma - \phi_0)) e^{2i\lambda_{\parallel}} + (1-r_0 \cos 2(\gamma - \phi_0)) e^{2i\lambda_{\perp}}}{\sqrt{\left(1+r_0^2 \cos^2 2(\gamma - \phi_0)\right) - \left(1-r_0^2 \cos^2 2(\gamma - \phi_0)\right) \cos 2(\lambda_{\parallel} - \lambda_{\perp})}} \end{aligned}$$

## APPENDIX C. INFINITESIMAL EVOLUTION AFTER INTERACTION

Within the context of the GLKS dynamical system it is interesting to examine the case of an infinitesimal variation of the density matrix of the light after interaction with the quantum polariser by allowing

the factor  $\cos(\lambda_{\parallel} - \lambda_{\perp})$  to vary with time as  $\approx 1 - \delta(t)$ ,  $\delta \ll 1$ . Then  $\cos^2(\lambda_{\parallel} - \lambda_{\perp}) \approx 1 - 2\delta$ , and we obtain for Eqs. (4.12) – (4.15):

$$(C.1) \quad r' \approx r_0(1 - \delta \sin^2 2(\gamma - \phi_0)) \approx r_0 \exp -\delta \sin^2 2(\gamma - \phi_0),$$

$$(C.2) \quad a \approx \cos 2\phi_0 - \delta \sin 2(\gamma - \phi_0) \sin 2\gamma,$$

$$(C.3) \quad b \approx \sin 2\phi_0 + \delta \sin 2(\gamma - \phi_0) \cos 2\gamma,$$

$$(C.4) \quad \tan \phi' \approx \tan \phi_0 + \delta \frac{\sin 2(\gamma - \phi_0)}{\sin 2\phi_0 \cos \phi_0} [(\sin(2\gamma - \phi_0) - \cos \phi_0 \sin 2(\gamma - \phi_0))].$$

Eq. (C.4) can be rewritten as

$$\tan \phi' - \tan \phi_0 \approx \frac{\phi' - \phi_0}{\cos^2 \phi_0} \approx \delta \frac{\sin 2(\gamma - \phi_0)}{\sin 2\phi_0 \cos \phi_0} [(\sin(2\gamma - \phi_0) - \cos \phi_0 \sin 2(\gamma - \phi_0))],$$

and so

$$(C.5) \quad \frac{\Delta \phi}{\delta} \approx \frac{\sin 2(\gamma - \phi_0)}{2 \sin \phi_0} [(\sin(2\gamma - \phi_0) - \cos \phi_0 \sin 2(\gamma - \phi_0))].$$

By comparing Eq. (C.1) and Eq. (C.5) with the GKLS equations Eq. (2.20) and Eq. (2.19) respectively in the case  $\alpha = 0$ , one can identify the parameters  $\delta$ ,  $\beta$ , and  $\mathcal{E}$ :

$$(C.6) \quad \delta(t) = t - t_0 = \Delta t \ll 1, \quad \beta = \sin^2 2(\gamma - \phi_0).$$

$$(C.7) \quad \mathcal{E} = -\frac{\sin 2(\gamma - \phi_0)}{2 \sin \phi_0} [(\sin(2\gamma - \phi_0) - \cos \phi_0 \sin 2(\gamma - \phi_0))].$$

**Acknowledgments.** We thank the financial support from the Brazilian scientific agencies Fundação de Amparo à Pesquisa do Estado do Rio de Janeiro (FAPERJ), Coordenação de Aperfeiçoamento de Pessoal de Nível Superior (CAPES) and Conselho Nacional de Desenvolvimento Científico e Tecnológico (CNPq), grant related to Programa de Capacitação Institucional (PCI) 2018-2023, number 301098/2024-7. T.K. acknowledges the financial support by CNPq (No. 305654/2021-7) and the Fueck-Stiftung. A part of this work has been done under the project INCT-Nuclear Physics and Applications (No. 464898/2014-5).

## REFERENCES

- [1] R. A. Jefferson and R. C. Myers, Circuit complexity in quantum field theory, *JHEP* **10** 107 (2017). [I](#)
- [2] L. Susskind, Computational Complexity and Black Hole Horizons, *Fortsch. Phys.* **64** 24 (2016). [I](#)
- [3] L. Susskind, Three Lectures on Complexity and Black Holes, arXiv:1810.11563v1 [hep-th]. [I](#)
- [4] M. A. Nielsen, A geometric approach to quantum circuit lower bounds, *Quant. Inf. Comput.* **6** 213-262 (2006). [I](#)
- [5] M. A. Nielsen, M. R. Dowling, M. Gu, A. M. Doherty, Quantum computation as geometry, *Science* **311** 1133 (2006). [I](#)
- [6] M. R. Dowling and M. A. Nielsen, The geometry of quantum computation, *Quantum Information and Computation* **8** (2008). [I](#)
- [7] R. J. Gordon and S. A. Rice, Active control of the dynamics of atoms and molecules, *Ann. Rev. Phys. Chem.* **48** 601 (1997). [I](#)
- [8] M. Shapiro and P. Brumer, *Principles of the quantum control of molecular processes*, Wiley-VCH, Germany, (2003). [I](#)
- [9] H. Rabitz, R. de Vivie-Riedle, M. Motzkus, and K. Kompa, Whither the future of controlling quantum phenomena?, *Science* **288** 824 (2000). [I](#)
- [10] S. Rice and M. Zhao, *Optimal control of quantum dynamics*, Wiley, U.S.A., (2000). [I](#)

- [11] H. Bergeron, E. Curado, J.-P. Gazeau, and L. Rodrigues, Orientations in the Plane as Quantum States, *Brazilian Journal of Physics* **49** 391-401 (2019). [1](#), [2.3.1](#)
- [12] R. Beneduci, E. Frion, J.-P. Gazeau, and A. Perri, Quantum formalism on the plane: POVM-Toeplitz quantization, Naimark theorem and linear polarisation of the light, *Annals of Physics* **447** 169134 (2022) [1](#)
- [13] M Naghiloo, D Tan, PM Harrington, JJ Alonso, E Lutz, A Romito, Heat and work along individual trajectories of a quantum bit, *Phys. Rev. Lett.* **124** 110604 (2020) [1](#)
- [14] J. von Neumann, *Mathematical Foundations of Quantum Mechanics*, Princeton Univ. Press, Princeton, N.J., 1955. [1](#)
- [15] A. Z. Goldberg, P. de la Hoz, G. Björk, A. B. Klimov, M. Grassl, G. Leuchs, and L. L. Sánchez-Soto, Quantum concepts in optical polarization, *Advances in Optics and Photonics* **13** 1-73 (2021). [1](#)
- [16] P. A. Mello, The von Neumann model of measurement in quantum mechanics, *AIP Conf. Proc.* **1575** 136-165 (2014). [1](#)
- [17] I. Bengtsson and K. Zyczkowski, *Geometry of Quantum States: An Introduction to Quantum Entanglement* (1st ed.), Cambridge University Press (2007) p. 301. [2.2](#)
- [18] D. Chruściński and S. Pascazio, A Brief History of the GKLS Equation, *Open Systems & Information Dynamics* **24** 1740001 (2017). [2.3.2](#), [6.1](#)
- [19] H.-P. Breuer and F. Petruccione, *The Theory of open quantum systems*, Oxford Univ Press, 2002. [2.3.2](#)
- [20] E. L. Ince, *Ordinary Differential Equations*, New York: Dover Publications, pp. 23-25, 1956. [2.3.2](#)
- [21] W. H. McMaster, Polarization and the Stokes Parameters, *Am. J. Phys.* **22** 351 (1954). [3](#)
- [22] B. Schaefer et al, Measuring the Stokes polarisation parameters, *Am. J. Phys.* **75** 163-168 (2007). [3](#)
- [23] E. M. Landau, *The Classical Theory of Fields*, Vol. 2 (4th ed.) Butterworth-Heinemann 1975. [3](#)
- [24] A. Peres, Neumark's Theorem and Quantum Inseparability, *Found. Phys.* **20** 1441-1453 (1990). [4.1](#)

- [25] R. Chipman, W. S. T. Lam, G. Young, *Polarized light and optical systems*, CRC Press 2018. 5
- [26] A. Rivas and S. F. Huelga, Time evolution in open quantum systems, in *Open Quantum Systems: An Introduction* SpringerBriefs in Physics, pp. 19–31 2012. 6.1
- [27] R. Alicki and K. Lendi, *Quantum dynamical semigroups and applications* Vol. 717, Springer Section 1.4.2 p. 20. 2007. 6.1
- [28] I. S. Gradshteyn, I. M. Ryzhik, *Table of integrals, series, and products*, (7th ed.) Academic press 2014. 7.1
- [29] A. Carlini, A. Hosoya, T. Koike, Y. Okudaira, Time–Optimal Quantum Evolution, *Phys. Rev. Lett.* **96** 060503 (2006). 9
- [30] T. Koike, Quantum brachistochrone, *Phil. Trans. R. Soc. A* **380** 20210273 (2022). 9
- [31] P. Kammerlander and J. Anders, Coherence and measurement in quantum thermodynamics. *Sci. Rep.* **6** 22174 (2016). 9
- [32] C. Elouard, D. A. Herrera-Martí, M. Clusel, A. Auffèves, The role of quantum measurement in stochastic thermodynamics, *npj Quantum Information* **3** 9 (2017). 9

<sup>A</sup> *CENTRO BRASILEIRO DE PESQUISAS FÍSICAS*,  
*RUA XAVIER SIGAUD 150, 22290-180, RIO DE JANEIRO, RJ, BRAZIL*

<sup>B</sup> *INSTITUTO NACIONAL DE CIÊNCIA E TECNOLOGIA, SISTEMAS COMPLEXOS*,  
*RUA XAVIER SIGAUD 150, 22290-180, RIO DE JANEIRO, RJ, BRAZIL*

<sup>C</sup> *UNIVERSIDADE FEDERAL FLUMINENSE*

<sup>D</sup> *UNIVERSITÉ PARIS CITÉ*,  
*CNRS, ASTROPARTICULE ET COSMOLOGIE*  
*75013 PARIS, FRANCE*

44 E. M.F. CURADO, S. FACI, J.-P. GAZEAU, T. KOIDE, A. C. MAIOLI, D. NOGUERA

<sup>E</sup> *INSTITUTO DE FÍSICA, UNIVERSIDADE FEDERAL DO RIO DE JANEIRO,*

*C.P. 68528, 21941-972, RIO DE JANEIRO, RJ, BRAZIL*

*Email address:* [evaldo@cbpf.br](mailto:evaldo@cbpf.br)

*Email address:* [sofiane.faci@gmail.com](mailto:sofiane.faci@gmail.com)

*Email address:* [gazeau@apc.in2p3.fr](mailto:gazeau@apc.in2p3.fr)

*Email address:* [tomoikoide@gmail.com](mailto:tomoikoide@gmail.com)

*Email address:* [alanmaioli@cbpf.br](mailto:alanmaioli@cbpf.br)

*Email address:* [diegonoguera.srl@gmail.com](mailto:diegonoguera.srl@gmail.com)